Near-ultraviolet absorption cross-sections of nitrophenols and their potential influence on tropospheric oxidation capacity

*Jun Chen, John C. Wenger and Dean S. Venables**

Department of Chemistry and Environmental Research Institute, University College Cork, Cork, Ireland

j.chen@student.ucc.ie, j.wenger@ucc.ie, d.venables@ucc.ie

*d.venables@ucc.ie

ABSTRACT

Nitrophenols and methyl-nitrophenols have been identified as photolytic precursors of nitrous acid, HONO, but their gas-phase absorption has not previously been reported. In this study, the absorption cross-sections of 2-nitrophenol, 3-methyl-2-nitrophenol, and 4-methyl-2-nitrophenol were measured from 320 to 450 nm using incoherent broadband cavity-enhanced absorption spectroscopy (IBBCEAS). The benzaldehyde absorption spectrum was measured to validate the approach and was in good agreement with literature spectra. The nitrophenol absorption cross-sections are large (ca. 10^{-17} cm^2 $molecule^{-1}$) and blue-shifted about 20 nm compared to previously measured solution spectra. Besides forming HONO, nitrophenol absorption influences other photochemistry by reducing the available actinic flux. The magnitudes of both effects are evaluated as a function of solar zenith angle, and nitrophenol absorption is shown to lower the photolysis rates of O_3 and NO_2.

KEYWORDS:

photolysis

benzaldehyde

broadband cavity-enhanced absorption spectroscopy

atmospheric simulation chamber

tropospheric oxidation

1. Introduction

Nitrophenols are an important class of carcinogenic and phytotoxic pollutants that have been the subject of environmental scrutiny since the 1970s.[1] Atmospheric sources of nitrophenols include primary emissions from vehicles and secondary formation from tropospheric reactions of mono-aromatic compounds with the hydroxyl radical, OH, in the presence of nitrogen oxides, or NO_3-initiated oxidation of phenol and cresols.[2-5] Lately, nitrophenols in the gas phase have attracted attention as photolytic precursors of nitrous acid, HONO,[6-7] an important tropospheric species which readily photolyzes to form OH, the principal oxidant in the atmosphere.[8-10] Following this discovery, other ortho-nitroaromatics have been shown to photolyze to HONO or OH.[11-12] The interest in nitrophenol photochemistry has also stimulated fundamental studies of the dynamics of the photodissociation process.[13-14] The photolysis rates of 2-nitrophenol and a number of methyl-2-nitrophenols have been measured in an indoor reactor and also at the outdoor chamber facility in Valencia, Spain.[6-7,15] The results indicate that photolysis is the dominant atmospheric loss process for these compounds, with lifetimes as short as 1 hour under conditions of high solar irradiance.[7] In order to calculate the photolysis rate under different atmospheric conditions, wavelength-dependent values of the absorption cross-section and quantum yield are required. However, the gas phase absorption spectra of nitrophenols have not yet been reported.

That there are no published gas phase spectra of the nitrophenols illustrates the general difficulty of measuring the absorption spectra of compounds with moderately low vapor pressure. Experimental challenges associated with compounds having sub-millibar vapor pressures at ambient temperatures include weak absorption, accurate quantification of the concentrations, and partitioning to the walls of the apparatus. Sensitive absorption measurements generally require long optical pathlengths through the sample and can be achieved using multipass cells or optical cavities. An optical cavity method that lends itself well to recording relatively broad spectra of weak absorptions is incoherent broadband cavity-

enhanced absorption spectroscopy (IBBCEAS),[16] in which a spectrograph measures the transmission of broadband light through an optical cavity. Previous work with broadband cavity systems has largely been applied to trace gas analysis, in which the reflectivity of the dielectric mirrors is usually maximized to increase the sensitivity of the system to small absorptions.[17-24] Prior studies have used bandwidths of 20 to 80 nm because increasing the reflectivity tends to narrow the high reflectivity region of the mirrors.[17,19] For measuring absorption cross-sections, on the other hand, it would be preferable to have a bandwidth sufficiently broad to cover the absorption band of the compound of interest. This is feasible with mirrors of lower reflectivity and in this paper we demonstrate an IBBCEAS system with a spectral window of around 130 nm, which we combine with an atmospheric simulation chamber as in prior work.[22-23,25] The low surface-to-volume ratios of such chambers are particularly suited to working with low vapor gases and aerosols as wall losses are greatly reduced and sample handling is simplified.

Our aim in this paper is to measure the near-ultraviolet absorption cross-sections of gas phase nitrophenols ($O_2NC_6H_4OH$) and methyl-2-nitrophenols ($CH_3C_6H_3(NO_2)OH$). We do so by applying an IBBCEAS system coupled across an atmospheric simulation chamber, which we propose as a convenient and robust method to measure the absorption cross-sections of low vapor pressure compounds. To validate the data analysis from the chamber measurements, we first compare our spectra of benzaldehyde (C_6H_5CHO), another relatively low vapor pressure compound of atmospheric importance, against published spectra. Finally, we evaluate the impact of near-UV absorption by nitrophenols on primary tropospheric photochemistry.

2. Experimental

The IBBCEAS spectrometer was coupled to an atmospheric simulation chamber in a similar manner to two previous studies.[22-23] The chamber was a 4.1 m long, flexible FEP bag with a diameter of approximately 1.1 m and an enclosed volume of approximately 3.9 m^3 at ambient pressure.[26] Rigid aluminum plates formed the ends of the chamber and the sides were enclosed by thin aluminum sheets to shield the chamber interior from ambient light. The end plates were covered with FEP-Teflon to reduce potential reactive losses of the chamber contents to metal surfaces. The chamber was purged with clean air from a Zander KMA 75 purification system for several hours (and usually overnight) before each experiment.

The optical cavity of the IBBCEAS system extended across the length of the chamber. Cavity mirrors (Layertec, 5.0 m radius of curvature) were housed in flexible mounts attached to each end of the chamber and were separated by 4.62 m. The average reflectivity of the mirrors was around 99.6% (manufacturer's specifications) over the high reflectivity region, which extended from approximately 300 to 450 nm. Each mirror was purged with purified air at 0.5 L min^{-1} to prevent deposition of particles and vapors onto the mirrors. The beam of a 75 W Xe arc lamp was directed into the optical cavity; light transmitted through the cavity was coupled into an Andor SR303 spectrograph with an iDus 420A-BU CCD detector, which was cooled to -40°C to reduce the dark current. The lamp was turned on and allowed to stabilize for at least an hour before each experiment. The integration time of each scan was 60 s. A combination of Schott BG3 and BG40 filters placed at the entrance to the cavity restricted the transmitted light of the lamp to between 320 and 450 nm. Such filtering is critical to prevent the very broadband output of the arc lamp (200 to 2000 nm) from adding to background light levels in the spectrograph. To observe the full spectrum through the cavity, a 150 l/mm grating with a 500 nm blaze wavelength was used; the modest resolution of the spectrograph (2.2 nm) was nevertheless suitable for the diffuse spectra reported here. The usable range of the spectrometer

extended from about 320 nm to 450 nm and the wavelength scale was calibrated using several emission lines from a Hg-Ar penray lamp. The uncertainty in the wavelength scale was 0.11 nm.

Samples and their purities were: benzaldehyde (Aldrich, >99%), 2-nitrophenol (Aldrich, 99%), 3-nitrophenol (Aldrich, 99%), 3-methyl-2-nitrophenol (Aldrich, 99%), 4-methyl-2-nitrophenol (Aldrich, 99%), and methyl vinyl ketone (Aldrich, 95%). All samples were used as received. Weighed samples were introduced into the chamber via an impinger connected to a stream of purified compressed air. The samples were volatilized into the carrier stream by gentle warming with a heat gun over a period of tens of seconds to several minutes, depending on the compound's volatility. The vapor pressures of these compounds at 20°C are 1.28 mbar (benzaldehyde),[27] 0.11 mbar (2-nitrophenol), 0.050 mbar (3-methyl-2-nitrophenol), and 0.046 mbar (4-methyl-2-nitrophenol).[28] The maximum mixing ratios of the compounds in the chamber were less than 1.8 ppmv (benzaldehyde), 90 ppbv (2-nitrophenol), and 42 ppbv (3-methyl-2-nitrophenol and 4-methyl-2-nitrophenol).

Calibration of the system:

The absorption coefficient α (or, more generally, the extinction coefficient ε) of a gaseous sample is given by:[16]

$$\alpha(\lambda) = \sum_i \sigma_i(\lambda) \cdot n_i / V = \frac{1}{d}\left(\frac{I_0(\lambda)}{I(\lambda)} - 1 \right)\left(1 - R(\lambda)\right) \qquad (1)$$

where I and I_0 are, respectively, the intensities transmitted through the optical cavity in the presence and absence of an absorber, d is the distance between the cavity mirrors, and R is the mirror reflectivity. The absolute absorption cross-section and number of molecules of species i are indicated by σ_i (cm^2 $molecule^{-1}$) and n_i, and V is the volume of the chamber (cm^{-3}). Equation (1) implies that the spectral dependence of the mirror reflectivity is required to quantify the sample absorption. Moreover, as the flexible FEP-Teflon bag expanded and contracted during the purging of the chamber, a modest variation

in the sample volume between experiments was expected. We therefore calibrated the product $V\cdot(1 - R)$ at the start of each experiment using a known mass of methyl vinyl ketone (MVK), which absorbs below 390 nm.[29] To extend the calibration to longer wavelengths, an arbitrary quantity of NO_2 was added to the chamber and $V\cdot(1 - R)$ was scaled accordingly at longer wavelengths.[30]

Figure 1(a) shows that the fractional absorption increases linearly with MVK mass at several wavelengths. Combined with the NO_2 absorption, the spectral dependence of $V\cdot(1 - R)$ is shown in Fig. 1(b). The useful spectral range of 320 to 450 nm is notably broader, and extends to shorter wavelengths, than prior studies using broadband cavity spectrometers.[17] Unlike most optical cavity mirrors, which have a relatively flat transmission minimum over the short range of high reflectivity, the calibrated mirror spectrum has obvious undulations. These are in good agreement with the scaled transmission spectra of the mirrors recorded by the manufacturer. Although the structures in the mirror spectrum could potentially influence the resulting absorption spectrum (cf. Eq. (1)),[19] we found no evidence that these features led to artifacts in the measured spectra. The uncertainty in $V\cdot(1 - R)$ was calculated to be 8% using standard error propagation, with contributory uncertainties arising from the sample mass (2%), MVK absorption cross-section at 360 nm (ca. 5%), cavity length (5%), and intensity measurement during the addition of MVK (2%).

Standard addition method

The long purge time of the atmospheric simulation chamber – a minimum of several hours – precludes measuring a single spectrum per experiment on practical grounds. However, if the chamber absorption is monitored continuously and no rapid changes occur in the sample absorption (from fast deposition to chamber surfaces or reactions within the chamber, for example), it is possible to carry out multiple absorption measurements during each chamber experiment by using a variation of the standard addition method.[31]

Consider the time-dependent nature of the absorption coefficient of the chamber constituents:

$$\alpha(t) = \left(\frac{I_0 - I(t)}{I(t)} \right) \left(\frac{1-R}{L} \right) \tag{2}$$

where I_0 is the intensity transmitted through the clean chamber and $I(t)$ is the intensity at the time of measurement. Adding an absorbing compound to the chamber increases the overall sample absorption, and the difference ($\Delta\alpha$) between the sample absorption before (α_B) and after (α_A) addition of the absorber is

$$\Delta\alpha = \alpha_A - \alpha_B \tag{3}$$

If I_B and I_A are the intensities measured before and after the addition, the change in the absorption in the chamber is then:

$$\Delta\alpha = \left[\left(\frac{I_0 - I_A}{I_A} \right) - \left(\frac{I_0 - I_B}{I_B} \right) \right] \left(\frac{1-R}{L} \right) = \left[\frac{I_0 (I_B - I_A)}{I_A I_B} \right] \left(\frac{1-R}{L} \right) \tag{4}$$

This result is not the same as assuming:

$$\Delta\alpha = \left(\frac{I_B - I_A}{I_A} \right) \left(\frac{1-R}{L} \right), \tag{5}$$

which does not take into account that the sample extinction shortens the effective pathlength of light in the cavity, as discussed by Platt *et al.*[32]

Figure 2 shows the stepwise drop in the intensity as an absorbing compound (2-nitrophenol in this case) was added to the chamber. The intensity stabilized within a minute or two of each sample addition, and losses to chamber surfaces are manifest as a slight, but increasingly positive slope as the concentration increased. The measurement of $\Delta\alpha$ was taken within a few minutes of adding the sample; wall losses during the sample addition period were small (below 1% of the observed change) and are ignored in our analysis. As I_0 must reasonably approximate the transmitted intensity of the clean

chamber at the time of both measurements, normalization is necessary if the lamp output varies significantly with time. The linear drop in the intensity before the first addition at around 1400 s was used as the basis for normalizing I_0 at later times. The rate of decrease was spectrally-dependent, with faster dimming at short rather than at long wavelengths. We estimate a conservative uncertainty of 10% in measuring the intensity decrease in Equation (4), which combined with the calibration and other sources of uncertainty gives an overall uncertainty of 14% (1 σ) around the maximum of the resulting cross-sections.

3. Results

Benzaldehyde

Benzaldehyde has a relatively low vapor pressure (1.28 mbar at 20°C) and its gas-phase absorption cross-section in the near-UV has previously been reported.[33-34] It was therefore selected as a test compound for validating our method. The absorption spectrum of benzaldehyde was recorded for masses of 3.8, 5.7, 8.8, and 12.6 mg introduced into the chamber, corresponding to increases in the mixing ratio of 0.22, 0.34, 0.52, and 0.74 ppmv. As with the MVK calibration of the mirror reflectivity spectrum, the absorption varied linearly with the amount of benzaldehyde in the chamber (Fig. 3a). The absorption cross-section of benzaldehyde recorded in the chamber is shown in Fig. 3b. The absorption extends to around 380 nm and several diffuse bands are apparent in the spectrum with maxima at 339 nm (29.5×10^3 cm^{-1}), 354 nm (28.3×10^3 cm^{-1}), and 371 nm (27.0×10^3 cm^{-1}), in good agreement with earlier high resolution studies.[35-36] These features are separated by 1250 to 1300 cm^{-1} and form part of a vibrational progression of the excited state carbonyl stretching mode.[35] A small offset of about 3×10^{-21} cm^2 molecule^{-1} is visible in our spectrum beyond 380 nm and probably arises from lamp dimming.

Our benzaldehyde absorption cross-section is in broad agreement with previous reports, also shown in Fig. 3. Thiault *et al.* used an elevated temperature and multipass cell arrangement while Xiang and co-workers used cavity ringdown measurements in a vacuum cell at room temperature.[33-34] The three spectra agree well below 360 nm. The spectrum of Thiault *et al.* has a similar magnitude and structure to ours, but their reported spectrum is blue shifted by about 4 nm relative to ours. As the vibrational structure in their spectrum is also inconsistent with earlier high-resolution spectra of benzaldehyde,[35-36] we accordingly show their shifted spectrum in Fig. 3. Shifting the wavelength also improves the agreement between their spectrum and that of Xiang *et al.* Fine structure is precluded from the Xiang spectrum where absorption cross-sections were reported every 5 nm. Their absorption cross-sections diverge significantly from our values and those Thiault *et al.* at 360 nm and 365 nm, where their cross-sections are larger by a factor of two to three. The source of this disagreement probably does not lie in the poorer signal-to-noise of the Thiault spectrum (as Xiang and co-workers suggest) because our cross-section in this region is similar to that of the (shifted) Thiault spectrum. In addition, high resolution spectra display no evidence for significant vibrational band contributions to the spectrum near 365 nm.[35-36] Either our cross-sections or those from the shifted spectrum of Thiault are probably marginally better for estimating photolysis rates of benzaldehyde in the atmosphere. This difference is relatively small: the integrated cross-sections of our work and the shifted Thiault spectrum are both ca. 10% lower than the cavity-ringdown spectrum of Xiang and colleagues and within the reported uncertainties of the three spectra. Aside from these minor differences between spectra, however, we conclude that the broadband cavity approach combined with the atmospheric simulation chamber produces reliable results.

2-Nitrophenol and methyl-2-nitrophenols

The near-UV absorption of nitrophenols arises from the π (benzene ring) → π* (nitro group) transition.[37] Although solution spectra of the nitrophenols are readily measured, we are not aware of any gas phase spectra of these compounds in the literature. The absorption of nitrophenols varied linearly with concentration and the resulting spectra are shown in Fig. 4. The solid line denotes the spectrum obtained from the linear regression of all four additions (where the uncertainty in the slope is approximately 5%). The absorption band of 2-nitrophenol peaks around 336 to 339 nm with a very large absorption cross-section of 1.76×10^{-17} cm^2 molecule^{-1} and an apparent halfwidth of around 40 nm. The shape of the long-wavelength tail of the absorption agrees with the photofragment excitation spectrum of Cheng and co-workers.[13] The short-wavelength limit of the spectrum extends slightly beyond the peak maximum, where the absorption appears to fall more rapidly than at longer wavelengths. Methyl substitution in the 3-position results in a 50% weaker absorption maximum. Although the maximum absorption occurs at the same wavelength as that of 2-nitrophenol, the absorption band of 3-methyl-2-nitrophenol is broader and extends to almost 420 nm. The absorption maximum of 4-methyl-2-nitrophenol occurs between 340 and 353 nm and similarly extends further into the visible than the 2-nitrophenol absorption.

Gentle shoulders on the absorption bands are apparent in the spectra of 2-nitrophenol and its methylated isomers. These spectral features are not artifacts of the mirror reflectivity: they coincide with neither the position nor separation of extrema in the mirror reflectivity spectrum (cf. Fig. 1); moreover, their locations differ slightly in the three nitrophenol spectra. Rather, the features probably indicate underlying vibronic structure, most likely from the symmetric or asymmetric stretch of the aryl-NO_2, which absorb strongly at 1325 cm^{-1} and 1550 cm^{-1} in the ground electronic state and are similar to the approximate 1300 to 1700 cm^{-1} separation of peaks observed here.[38-39] The corresponding solution spectra are also included in Fig. 4. The spectra were recorded in acetonitrile, although there is little difference between spectra in acetonitrile, methanol, or 1-propanol.[15] The absorption peaks of the

solution spectra are red-shifted by 10 to 20 nm compared to the gas-phase spectra and the solution spectra also extend 20 to 40 nm further towards longer wavelengths.

Reported photolysis rates of the nitrophenols are modest for such large absorption cross-sections and the quantum yields of photolysis are correspondingly small.[6,15] We recalculated the average photolysis quantum yield of 2-nitrophenol based on the simulation chamber measurements of Bardini and the gas phase absorption cross-sections reported above. The absorption cross-section was linearly extrapolated from the experimental value at 320 nm to zero at 300 nm; deviations from this assumed absorption profile will little influence the final result as the photon flux is small in this region. Bardini reported a 2-nitrophenol photolysis rate of 0.63×10^{-4} s^{-1} when exposed to natural sunlight in the EUPHORE chamber (Valencia, Spain): the experiment was conducted around noon on 25 November when the solar zenith angle was approximately 60° and the average $J(NO_2)$ value was 4.56×10^{-3} s^{-1} (calculated from spectroradiometer measurements). Cyclohexane was added to the chamber as a scavenger for OH radicals. Based on this measured 2-nitrophenol photolysis rate, and scaling the measured $J(NO_2)$ values to those calculated for best estimate actinic flux data,[40] the spectrally-averaged quantum yield of 2-nitrophenol photolysis is 11.5×10^{-4}. This revised quantum yield is larger than Bardini's value of 7.0×10^{-4} s^{-1} based on the solution phase absorption cross-section. This difference is expected as the broader, red-shifted solution cross-section overlaps more with the higher actinic flux at longer wavelengths. The new quantum yield is also much larger than the HONO quantum yield reported by Bejan for 3-methyl-2-nitrophenol (1.5×10^{-4} s^{-1}) from their photoreactor measurements. In this case, we note that that photolysis rates from the two studies differ significantly; further work is required to resolve these discrepancies and to determine the wavelength-dependence of photolysis.

We also attempted to measure the absorption spectra of 3- and 4- nitrophenol. Sample handling was much more problematic for these two compounds because their vapor pressures are markedly lower than

that of 2-nitrophenol owing to strong intermolecular hydrogen bonding.[38,41-42] Extensive, vigorous heating of these isomers in the inlet air stream resulted in some thermal decomposition and particle formation. Rapid deposition to chamber walls was also observed. Nevertheless, we include an arbitrarily-scaled spectrum of 3-nitrophenol: given the uncertainties arising from sample handling, this spectrum should be regarded as indicative only. In particular, a constant offset at long wavelengths suggests that particle formation contributed to the total sample extinction. Subtracting the long-wavelength extinction gives a spectrum which again is blue-shifted relative to the solution spectrum of 3-nitrophenol and is shown in Fig. 4d. An absorption spectrum of 4-nitrophenol could not be retrieved with any certainty.

4. Atmospheric implications and applications

Near-ultraviolet absorption by nitrophenols and methyl-nitrophenols influences the oxidizing capacity of the polluted troposphere in two ways. First, photolytic formation and subsequent photolysis of HONO produces the hydroxyl radical:

$$\text{HONO} + h\nu\ (< 400\ \text{nm}) \rightarrow \text{OH} + \text{NO} \qquad (6)$$

With its relatively long wavelength absorption and high photolysis quantum yield, HONO is particularly important in initiating daytime oxidation chemistry. From their photoreactor results for 3-methyl-2-nitrophenol, Bejan estimated a photolytic HONO formation rate of 100 pptv h^{-1} in the atmosphere assuming a concentration of all nitrophenols of 1 ppbv when $J(NO_2) = 0.01\ s^{-1}$.[6] Although probably not the largest atmospheric source of HONO, at these concentrations nitrophenol photolysis would contribute significantly to the estimated HONO production rate of 500 pptv h^{-1}.[11]

A second, opposite influence on atmospheric oxidizing capacity is that nitrophenol absorption may lower the actinic flux and thereby slow primary photochemical processes. Such absorption can indeed

be significant: for instance, the same 1 ppbv of nitrophenols would reduce the light transmitted through a 1 km column by about 3% near the absorption maximum of 340 nm. As has been found for particle absorption in aerosols in Mexico City and Los Angeles,[43-45] absorption in the near-UV is likely to reduce photochemical production of OH via photolysis of O_3

$$O_3 + h\nu\ (< 340\ \text{nm}) \rightarrow O_2 + O\ (^1D) \quad (7)$$

$$O\ (^1D) + H_2O \rightarrow 2\ OH \quad (8)$$

as well as tropospheric formation of O_3 by way of NO_2 photolysis at longer wavelengths:

$$NO_2 + h\nu\ (< 420\ \text{nm}) \rightarrow NO + O\ (^3P) \quad (9)$$

$$O\ (^3P) + O_2 \rightarrow O_3 \quad (10)$$

Photolysis rate coefficients of reactions (7) and (9) are denoted by $J(O^1D)$ and $J(NO_2)$, respectively. The effect of absorption will be greatest at large solar zenith angles when the air mass is large and, in the case of $J(O^1D)$, when the actinic flux below 320 nm is small.

The influence of nitrophenol absorption on $J(O^1D)$ and $J(NO_2)$ at different solar zenith angles was calculated for a 1 km high polluted boundary layer containing 1 ppbv of total nitrophenols (based on the 2-nitrophenol gas phase absorption) (Fig. 5a). The nitrophenol absorption cross-section was extrapolated linearly to zero at 300 nm as in Section 3. When the sun is overhead, both $J(O^1D)$ and $J(NO_2)$ decrease by about 1.5%, which is a significant proportion of the modeled 5 – 8% decrease in O_3 concentrations around Los Angeles arising from aerosol absorption and scattering.[44] Both rate coefficients drop at large solar zenith angles, with a steeper falloff observed for $J(O^1D)$; in contrast, the difference between the rate coefficients with and without nitrophenol absorption ($\Delta J = J_{NP} - J_0$) changes more gradually with the solar zenith angle. At 86°, for instance, $J(NO_2)$ is 13% lower when absorption is included while $J(O^1D)$ declines by 34% (Fig. 5b). The latter value should be treated with caution because of the assumed nitrophenol absorption in the critical region around 310 nm that contributes most to O_3 photolysis.

Nitrophenol absorption will thus dampen (and in effect delay) other daytime oxidation chemistry in the atmosphere, most obviously in winter and around sunrise and sunset. The effect is likely to be enhanced in the morning following nocturnal nitration of aromatics via NO_3 radical reactions.[4] The balance between the opposite contributions of 2-nitrophenol to the formation of OH is presented in Fig. 6, where the photolysis rate of 2-nitrophenol is compared to the decrease in $J(O^1D)$ from nitrophenol absorption. Nitrophenol photolysis makes the larger contribution to OH concentrations throughout the day; nonphotolytic absorption attenuates the O_3 photolysis rate at about 40% of that rate. Only at very large solar zenith angles does the (negative) absorption contribution approach that of the (positive) contribution from nitrophenol photolysis (Fig. 6b). The general effect of 2-nitrophenol is therefore to increase the oxidizing capacity of the troposphere during daylight hours.

Two comments on the above calculations are necessary. Firstly, the calculations were based on the assumption of Bejan et al. that the mixing ratio for all nitrophenols is 1 ppbv.[11] Although measurements of gas-phase nitrophenols in air are somewhat limited, the maximum mixing ratios observed for nitrophenols are around 0.03 ppbv for 2- and 4-nitrophenol,[46,47] indicating that this estimate is too high even when the methyl-nitrophenols and dinitrophenols are taken into account. On this basis, the effect of nitrophenol absorption is expected to be much less than calculated above. On the other hand, the actual gas phase cross-sections in the photochemically critical region around 310 nm may be much larger than we assumed. In particular, the stronger $\pi \rightarrow \pi^*$ transition of the aromatic ring starts near this wavelength and would greatly increase the total absorption. In addition, absorption maxima of 2,4-dinitrophenol, 4-nitrophenol, and its methyl-substituted congeners all occur close to 310 nm and are stronger (in aqueous solution) than that of 2-nitrophenol.[28] All these compounds have been found in the gas phase in significant concentrations.[46-49] The above considerations could therefore still have a

marked influence on $J(O^1D)$, although the influence of the nitrophenols on NO_2 photolysis is likely to be minor.

The question remains as to the extent to which other relatively involatile organic compounds contribute to gas-phase absorption in the near-ultraviolet and their influence on tropospheric photochemistry. As this study shows, such absorption can be considerable for nitrated aromatic compounds. Jacobson tabulated a large number of potentially absorbing compounds based on the composition of Los Angeles aerosol.[50] In addition to the nitrophenols and other nitrated aromatics, these compounds included various benzaldehydes, benzoic acids, phenols, and some polycyclic aromatic hydrocarbons. Many of these compounds absorb strongly in solution but the near-UV gas phase spectra are not known. Further spectral measurements are therefore required to record the near-UV absorption cross-sections of these and other relevant compounds, which may combine into a strongly absorbing cocktail in the lower troposphere.

This work also presents a new application of the broadband cavity technique. Although similar spectrometers using flow cells have report new absorption spectra of weakly absorbing compounds,[51-52] this is the first time the IBBCEAS approach has been used to measure the absorption spectra of relatively low volatility compounds. The spectrometer extended to shorter wavelengths and had a larger bandwidth than has hitherto been reported, and now covers most of the important actinic wavelengths in the troposphere. The method was validated by the good overall agreement between our absorption cross-section spectrum of benzaldehyde and those previously reported in the literature. Based on the vapor pressures of the compounds studied here, the simulation chamber spectrometer should be able to measure the spectra of substances with room temperature vapor pressures above approximately 10^{-2} mbar. Besides its application to such gases, the chamber is also suited to the study of the formation, growth, and aging of atmospheric particles. In this regard, we have recently applied this system to study

the optical properties of secondary organic aerosols in the near-UV. Little is known about aerosol properties in this spectral region, although several recent studies have suggested that particle absorption increases strongly at sub-visible wavelengths.[53-55]

5. Conclusions

A broadband cavity absorption spectrometer has been coupled to an atmospheric simulation chamber to measure the gas phase absorption cross-section spectra of 2-nitrophenol, 3-methyl-2-nitrophenol, and 4-methyl-2-nitrophenol for the first time. The compounds absorb strongly, with absorption maxima ranging from 0.9 to 1.8×10^{-17} cm^2 $molecule^{-1}$ at the absorption maxima near 340 nm. The gas phase absorption is blue-shifted by about 20 nm compared to solution spectra . The spectrum of benzaldehyde was also measured and is in good agreement with previous studies. Implications for atmospheric oxidation processes, via either photolysis to HONO or absorption of the available actinic flux, were evaluated. This work also extends the IBBCEAS technique further into the ultraviolet, and across a wider spectral window, than previously demonstrated. The coupling of the spectrometer across the large volume, low surface area of the simulation chamber is particularly suited to recording the gas phase spectra of low volatility atmospheric species, many of which have yet to be measured.

ACKNOWLEDGMENT

The authors thank Andy Ruth for loan of the cavity mirror mounts, Perla Bardini for recording the solution phase spectra, and Iusti Bejan for assistance with the atmospheric simulation chamber. This material is based upon works supported by the Science Foundation Ireland under Grant No. 06/RFP/CHP055 and the EU FP7 project EUROCHAMP2 (grant no. 228335).

SUPPORTING INFORMATION AVAILABLE

Tabulated absorption cross-sections of benzaldehyde, 2-nitrophenol, 3-methyl-2-nitrophenol, and 4-methyl-2-nitrophenol from 320 to 450 nm. This material is available free of charge via the Internet at http://pubs.acs.org.

FIGURE CAPTIONS

Figure 1. Calibration of the spectrometer: (a) Fractional absorption for individual additions of methyl vinyl ketone (MVK) to the chamber at 340 nm (black), 350 nm (red), 360 nm (blue), and 370 nm (green). (b) The calibration of $V \cdot (1 - R)$ using NO_2 (blue line) after scaling to the calibration based on the MVK absorption at 360 nm (red triangle). Also shown is the arbitrarily-scaled manufacturer's transmission spectrum (black circles).

Figure 2. Changes in the intensity at 340 nm for several successive additions of 2-nitrophenol. Black circles are the original data, the dashed black line shows the extrapolated I_0, and the dashed red lines are the normalized data.

Figure 3. (a) The fractional absorption at four wavelengths with increasing mass of benzaldehyde. (b) The benzaldehyde absorption cross-section from this work and from the literature. Note that the spectrum of Thiault et al. was shifted by 4 nm to longer wavelengths (see text).

Figure 4. Absorption cross-sections in the gas phase (black lines) and acetonitrile solution (blue dashes): (a) 2-nitrophenol (b) 3-methyl-2-nitrophenol (c) 4-methyl-2-nitrophenol and (d) 3-nitrophenol (arbitrarily scaled).

Figure 5. (a) Variation with solar zenith angle of $J(NO_2)$, $J(O^1D)$ and the photolysis rate coefficient of 2-nitrophenol, J(2NP). The effect of absorption on $J(NO_2)$ and $J(O^1D)$ by 1 ppbv of 2-nitrophenol in a 1 km high boundary layer is also considered: ΔJ (dotted lines) denotes the difference

between the corresponding rate coefficient with and without nitrophenol absorption. (b) The dependence on the solar zenith angle of the fractional decrease in $J(NO_2)$ and $J(O^1D)$ caused by nitrophenol absorption.

Figure 6. (a) Influence of nitrophenol absorption on the OH formation rate where conditions of 50 ppbv O_3, 2-nitrophenol at 1 ppbv (in a 1 km high boundary layer), and 50% relative humidity have been assumed. The red dots indicate the upper limit for the formation rate of OH (via HONO) from the direct photolysis of 2-nitrophenol. The rate of formation of OH from O_3 photolysis is shown as the black squares, while the green squares indicate the extent to which nitrophenol absorption suppresses OH production via O_3 photolysis. (b) The ratio of the nitrophenol absorption effect to the nitrophenol photolysis on OH formation rates.

FIGURES

Figure 1.

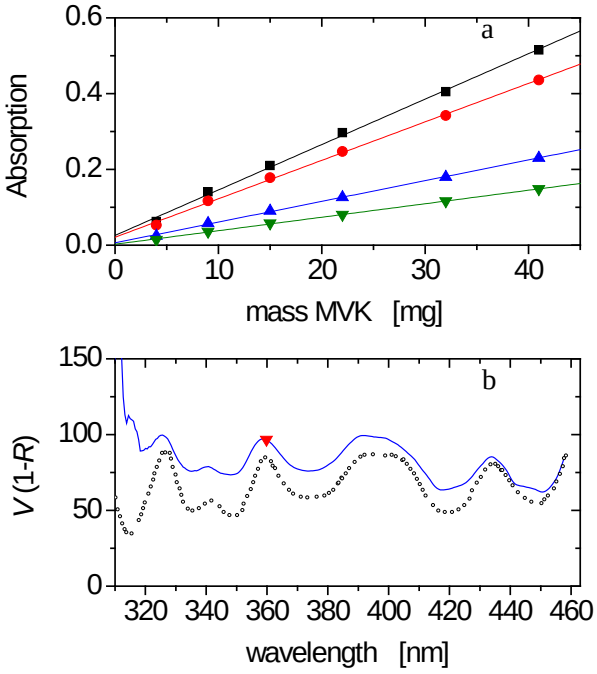

Figure 2.

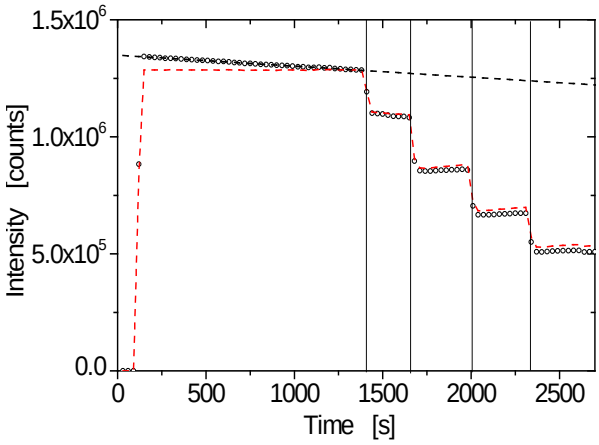
1.5x10^6
1.0x10^6
5.0x10^5
0.0
Intensity [counts]
0
500
1000
1500
2000
2500
Time [s]

Figure 3.

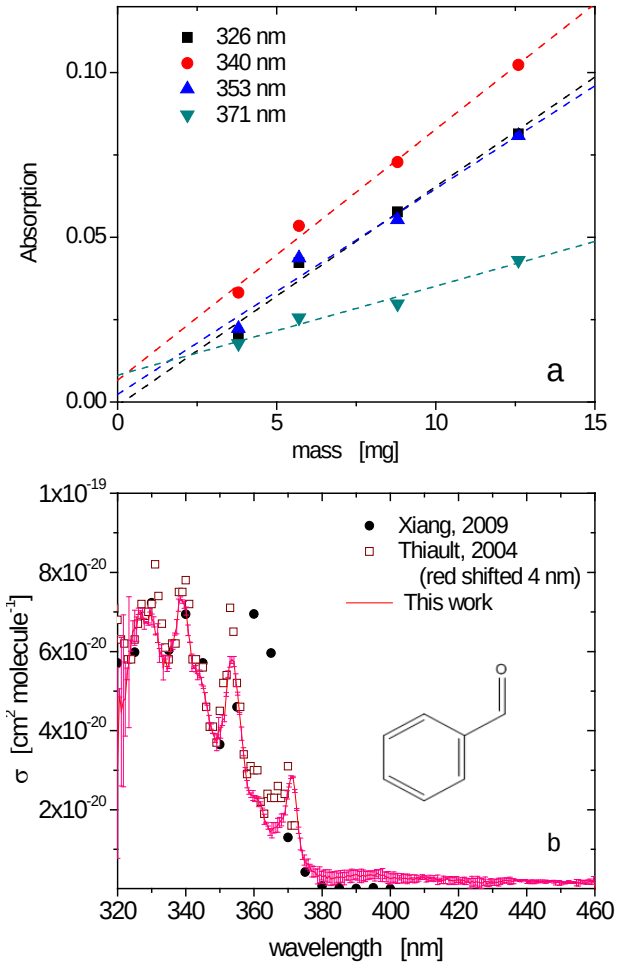
326 nm
340 nm
353 nm
371 nm
Absorption
0.10
0.05
0.00
0
5
10
15
mass [mg]
a
1x10-19
8x10-20
6x10-20
4x10-20
2x10-20
σ [cm2 molecule-1]
Xiang, 2009
Thiault, 2004
(red shifted 4 nm)
This work
O
b
320
340
360
380
400
420
440
460
wavelength [nm]

Figure 4.

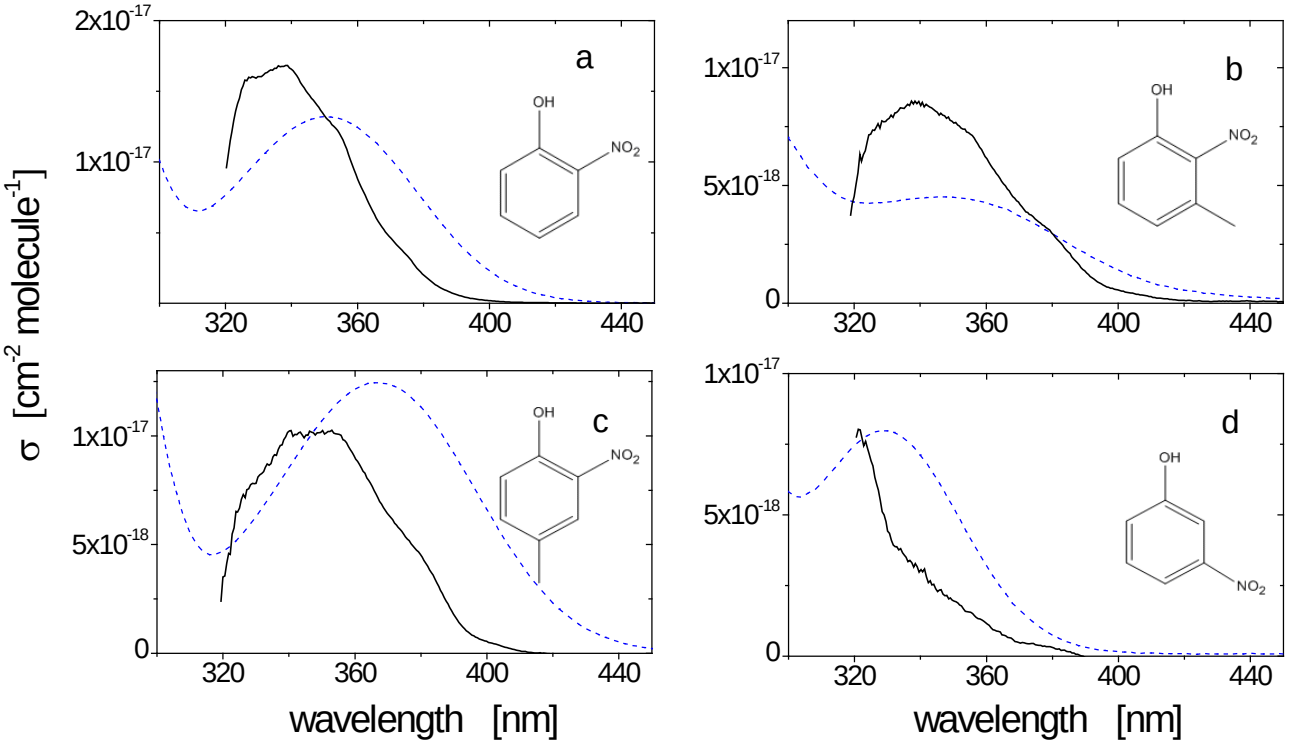
σ [cm-2 molecule-1]
2x10-17
1x10-17
0
5x10-18
320
360
400
440
wavelength [nm]
a
b
c
d
OH
NO2

Figure 5.

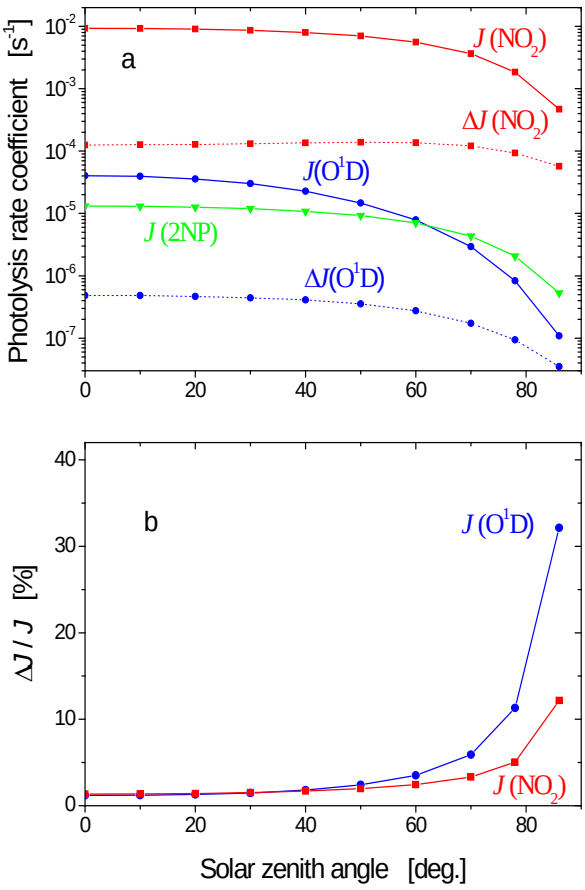
a
b
Photolysis rate coefficient [s-1]
ΔJ / J [%]
Solar zenith angle [deg.]
J (NO2)
ΔJ (NO2)
J(O1D)
J (2NP)
ΔJ(O1D)
J (O1D)
J (NO2)

Figure 6.

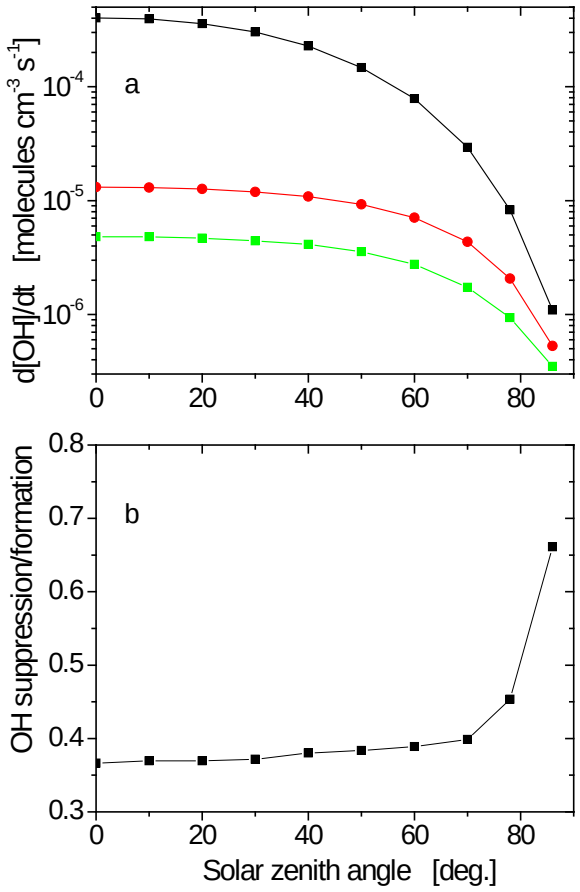
a
b
d[OH]/dt [molecules cm-3 s-1]
OH suppression/formation
Solar zenith angle [deg.]
10-4
10-5
10-6
0.8
0.7
0.6
0.5
0.4
0.3
0
20
40
60
80

REFERENCES

(1) Harrison, M. A. J.; Barra, S.; Borghesi, D.; Vione, D.; Arsene, C.; Olariu, R. L. *Atmos. Environ.* **2005**, *39*, 231-248.

(2) Tremp,.J.; Mattrel, P.; Fingler, S.; Giger, W. *Water Air and Soil Pollut.* **1993**, *68*, 113-123.

(3) Bolzacchini, E.; Bruschi, M.; Hjorth, J.; Meinardi, S.; Orlandi, M.; Rindone, B.; Rosenbohm, E. *Environ. Sci. Technol.* **2001**, *35*, 1791-1797.

(4) Atkinson, R.; Aschmann, S. M.; Arey, J. *Environ. Sci. Technol.* **1992**, *26*, 1397-1403.

(5) Olariu, R. I.; Klotz, B.; Barnes, I.; Becker, K. H.; Mocanu, R. *Atmos. Environ.* **2002**, *36*, 3685-3697.

(6) Bejan, I.; Abd El Aal, Y.; Barnes, I.; Benter, T.; Bohn, B.; Wiesen, P.; Kleffmann, J. *Phys. Chem. Chem. Phys.* **2006**, *8*, 2028-2035.

(7) Bejan, I.; Barnes, I.; Olariu, R.; Zhou, S. M.; Wiesen, P.; Benter, T. *Phys. Chem. Chem. Phys.* **2007**, *9*, 5686-5692.

(8) Ammann, M.; Kalberer, M.; Jost, D. T.; Tobler, L.; Rössler, E.; Piguet, D.; Gäggeler, H. W.; Baltensperger, U. *Nature* **1998**, *395*, 157-160.

(9) Aubin, D. G.; Abbatt, J. P. D. *J. Phys. Chem. A* **2007**, *111*, 6263-6273.

(10) Stemmler, K.; Ammann, M.; Donders, C.; Kleffmann, J.; George, C. *Nature* **2006**, *440*, 195-198.

(11) Kleffmann, J. *Chemphyschem* **2007**, *8*, 1137-1144.

(12) SenGupta, S.; Upadhyaya, H. P.; Kumar, A.; Dhanya, S.; Naik, P. D.; Bajaj, P. *Chem. Phys. Lett.* **2008**, *452*, 239-244.

(13) Cheng, S. B.; Zhou, C. H.; Yin, H. M.; Sun, J. L.; Han, K. L. *J. Chem. Phys.* **2009**, *130*, 234311.

(14) Han, K. L.; Wei, Q.; Yin, H. M.; Sun, J. L.; Yue, X. F. *Chem. Phys. Lett.* **2008**, *463*, 340-344.

(15) Bardini, P. Atmospheric chemistry of dimethylphenols and nitrophenols. PhD, University College Cork, 2006.

(16) Fiedler, S. E.; Hese, A.; Ruth, A. A. *Chem. Phys. Lett.* **2003**, *371*, 284-294.

(17) Thalman, R.; Volkamer, R. *Atmos. Meas. Tech.* **2010**, *3*, 1797-1814.

(18) Langridge, J. M.; Ball, S. M.; Shillings, A. J. L.; Jones, R. L. *Rev. Sci. Instrum.* **2008**, *79*, 123110.

(19) Triki, M.; Cermak, P.; Mejean, G.; Romanini, D. *Appl. Phys. B-Lasers Opt.* **2008**, *91*, 195-201.

(20) Washenfelder, R. A.; Langford, A. O.; Fuchs, H.; Brown, S. S. *Atmos. Chem. Phys.* **2008**, *8*, 7779-7793.

(21) Fuchs, H.; Ball, S. M.; Bohn, B.; Brauers, T.; Cohen, R. C.; Dorn, H. P.; Dubé, W. P.; Fry, J. L.; Häseler, R.; Heitmann, U. et al. *Atmos. Meas. Tech.* **2010**, *3*, 21-37.

(22) Gherman, T.; Venables, D. S.; Vaughan, S.; Orphal, J.; Ruth, A. A. *Environ. Sci. Technol.* **2008**, *42*, 890-895.

(23) Venables, D. S.; Gherman, T.; Orphal, J.; Wenger, J. C.; Ruth, A. A. *Environ. Sci. Technol.* **2006**, *40*, 6758-6763.

(24) Kennedy, O. J.; Ouyang, B.; Langridge, J. M.; Daniels, M. J. S.; Bauguitte, S.; Freshwater, R.; McLeod, M. W.; Ironmonger, C.; Sendall, J.; Norris, O. et al. *Atmos. Meas. Tech.* **2011**, *4*, 1759-1776.

(25) Varma, R. M.; Venables, D. S.; Ruth, A. A.; Heitmann, U.; Schlosser, E.; Dixneuf, S. *Appl. Opt.* **2009**, *48*, B159-B171.

(26) Thüner, L. P.; Bardini, P.; Rea, G. J.; Wenger, J. C. *J. Phys. Chem. A* **2004**, *108*, 11019-11025.

(27) Demare, G. R.; Lehman, T.; Termonia, M. *J. Chem. Thermodyn.* **1973**, *5*, 829-832.

(28) Schwarzenbach, R. P.; Stierli, R.; Folsom, B. R.; Zeyer, J. *Environ. Sci. Technol.* **1988**, *22*, 83-92.

(29) Gierczak, T.; Burkholder, J. B.; Talukdar, R. K.; Mellouki, A.; Barone, S. B.; Ravishankara, A. R. *J. Photochem. Photobiol., A* **1997**, *110*, 1-10.

(30) Voigt, S.; Orphal, J.; Burrows, J. P. *J. Photochem. Photobiol., A* **2002**, *149*, 1-7.

(31) Skoog, A. A. W., D.M.; Holler, F.J. *Fundamentals of Analytical Chemistry, 5th ed.*; Saunders: New York, 1988.

(32) Platt, U.; Meinen, J.; Pohler, D.; Leisner, T. *Atmos. Meas. Tech.* **2009**, *2*, 713-723.

(33) Thiault, G.; Mellouki, A.; Le Bras, G.; Chakir, A.; Sokolowski-Gomez, N.; Daumont, D. *J. Photochem. Photobiol., A* **2004**, *162*, 273-281.

(34) Xiang, B.; Zhu, C. Z.; Zhu, L. *Chem. Phys. Lett.* **2009**, *474*, 74-78.

(35) Ohmori, N.; Suzuki, T.; Ito, M. *J. Phys. Chem.* **1988**, *92*, 1086-1093.

(36) Imanishi, S.; Semba, K.; Ito, M.; Anno, T. *Bull. Chem. Soc. Jpn.* **1952**, *25*, 150-153.

(37) Wang, Y.; Wang, H.; Zhang, S.; Pei, K.; Zheng, X.; Phillips, D.L. *J. Chem. Phys.* **2006**, *125*, 214506.

(38) Kovacs, A.; V, I.; Keresztury, G.; Pongor, G. *Chem. Phys.* **1998**, *238*, 231-243.

(39) Brown, D. W.; Floyd, A. J.; Sainbury, M. *Organic Spectroscopy*; John Wiley: Chicester, 1988.

(40) Finlayson-Pitts, B. J.; Pitts, J. N. *Chemistry of the upper and lower atmosphere : theory, experiments, and applications*; Academic Press: San Diego, 2000.

(41) Chen, P. C.; Chen, S. C. *Int. J. Quantum Chem.* **2001**, *83*, 332-337.

(42) Chen, P. C.; Lo, W.; Tzeng, S. C. *THEOCHEM* **1998**, *428*, 257-266.

(43) Li, G.; Bei, N.; Tie, X.; Molina, L. T. *Atmos. Chem. Phys.* **2011**, *11*, 5169-5182.

(44) Jacobson, M. Z. *J. Geophys. Res.* **1998**, *103*, 10593-10604.

(45) Dickerson, R. R.; Kondragunta, S.; Stenchikov, G.; Civerolo, K. L.; Doddridge, B. G.; Holben, B. N. *Science* **1997**, *278*, 827-830.

(46) Belloli, R.; Barletta, B.; Bolzacchini, E.; Meinardi, S.; Orlandi, M.; Rindone, B. *J. Chromatogr., A* **1999**, *846*, 277-281.

(47) Cecinato, A.; Di Palo, V.; Pomata, D.; Sciano, M. C. T.; Possanzini, M. *Chemosphere* **2005**, *59*, 679-683.

(48) Morville, S.; Scheyer, A.; Mirabel, P.; Millet, M. *Environ. Sci. Pollut. R.* **2006**, *13*, 83-89.

(49) Lüttke, J.; Scheer, V.; Levsen, K.; Wünsch, G.; Cape, J. N.; Hargreaves, K. J.; Storeton-West, R. L.; Acker, K.; Wieprecht, W. et al. *Atmos. Environ.* **1997**, *31*, 2637-2648.

(50) Jacobson, M. Z. *J. Geophys. Res.* **1999**, *104*, 3527-3542.

(51) Chen, J.; Venables, D. S. *Atmos. Meas. Tech.* **2011**, *4*, 425-436.

(52) Axson, J. L.; Washenfelder, R. A.; Kahan, T. F.; Young, C. J.; Vaida, V.; Brown, S. S. *Atmos. Chem. Phys. Discuss.* **2011**, *11*, 21655-21676.

(53) Chen, Y.; Bond, T. C. *Atmos. Chem. Phys.* **2010**, *10*, 1773-1787.

(54) Andreae, M. O.; Gelencser, A. *Atmos. Chem. Phys.* **2006**, *6*, 3131-3148.

(55) Martins, J. V.; Artaxo, P.; Kaufman, Y. J.; Castanho, A. D.; Remer, L. A. *Geophys. Res. Lett.* **2009**, *36*, doi: 10.1029/2009gl037435.

TOC IMAGE